The Astrophysical Journal Letters, 921:L8 (9pp), 2021 November 1 https://doi.org/10.3847/2041-8213/ac1f92
© 2021. The American Astronomical Society. All rights reserved.

Unveiling Shrouded Oceans on Temperate sub-Neptunes via Transit Signatures of Solubility Equilibria versus Gas Thermochemistry

Renyu Hu[1,2], Mario Damiano[1], Markus Scheucher[1,3], Edwin Kite[4], Sara Seager[5,6,7], and Heike Rauer[3,8]
[1] Jet Propulsion Laboratory, California Institute of Technology, Pasadena, CA 91109, USA; renyu.hu@jpl.nasa.gov
[2] Division of Geological and Planetary Sciences, California Institute of Technology, Pasadena, CA 91125, USA
[3] Institut für Planetenforschung, Deutsches Zentrum für Luft- und Raumfahrt, D-12489 Berlin, Germany
[4] Department of the Geophysical Sciences, University of Chicago, Chicago, IL 60637, USA
[5] Department of Earth, Atmospheric, and Planetary Sciences, Massachusetts Institute of Technology, Cambridge, MA 02139, USA
[6] Department of Physics and Kavli Institute for Astrophysics and Space Research, Massachusetts Institute of Technology, Cambridge, MA 02139, USA
[7] Department of Aeronautics and Astronautics, Massachusetts Institute of Technology, Cambridge, MA 02139, USA
[8] Institut für Geologische Wissenschaften, Freie Universität Berlin, D-12249 Berlin, Germany
Received 2021 July 28; revised 2021 August 10; accepted 2021 August 15; published 2021 October 28

Abstract

The recent discovery and initial characterization of sub-Neptune-sized exoplanets that receive stellar irradiance of approximately Earth's raised the prospect of finding habitable planets in the coming decade, because some of these temperate planets may support liquid-water oceans if they do not have massive H_2/He envelopes and are thus not too hot at the bottom of the envelopes. For planets larger than Earth, and especially planets in the 1.7–3.5 $R_\oplus$ population, the mass of the H_2/He envelope is typically not sufficiently constrained to assess the potential habitability. Here we show that the solubility equilibria versus thermochemistry of carbon and nitrogen gases typically results in observable discriminators between small H_2 atmospheres versus massive ones, because the condition to form a liquid-water ocean and that to achieve the thermochemical equilibrium are mutually exclusive. The dominant carbon and nitrogen gases are typically CH_4 and NH_3 due to thermochemical recycling in a massive atmosphere of a temperate planet, and those in a small atmosphere overlying a liquid-water ocean are most likely CO_2 and N_2, followed by CO and CH_4 produced photochemically. NH_3 is depleted in the small atmosphere by dissolution into the liquid-water ocean. These gases lead to distinctive features in the planet's transmission spectrum, and a moderate number of transit observations with the James Webb Space Telescope should tell apart a small atmosphere versus a massive one on planets like K2-18 b. This framework thus points to a way to use near-term facilities to constrain the atmospheric mass and habitability of temperate sub-Neptune exoplanets.

Unified Astronomy Thesaurus concepts: Exoplanet atmospheres (487); Extrasolar rocky planets (511); Extrasolar ice giants (2024); Habitable planets (695); Ocean planets (1151); Transmission spectroscopy (2133)

1. Introduction

The exoplanet community already has ways to detect an H_2 atmosphere by transmission spectroscopy via its pressure scale height 1 order of magnitude larger than that of an N_2 or CO_2 atmosphere (Miller-Ricci et al. 2008). However, the mass of the H_2 atmosphere—the parameter that controls the temperature at the bottom of the atmosphere and thus the possibility for liquid water (Pierrehumbert & Gaidos 2011; Ramirez & Kaltenegger 2017; Koll & Cronin 2019)—is not directly measurable from the transmission spectrum. Also, a planet's mass and radius typically allow multiple models of the interior structure (e.g., Rogers & Seager 2010; Valencia et al. 2013). It is unclear whether the planets in the 1.7–3.5 $R_\oplus$ population (Fulton & Petigura 2018) are mostly rocky planets with massive H_2/He gas envelopes (Owen & Wu 2017; Jin & Mordasini 2018) or planets with a massive water layer (∼50 wt%) that do not require a large H_2 envelope to explain their radius (e.g., referred to as "ocean planets" hereafter; Zeng et al. 2019; Mousis et al. 2020; Venturini et al. 2020). Direct-imaging observations in the future may provide means to detect a surface underneath a thin atmosphere on temperate planets, via the ocean glint (Robinson et al. 2010) or surface heterogeneity (Cowan et al. 2009; Fan et al. 2019). However, these methods are not applicable to the near-term capabilities such as the James Webb Space Telescope (JWST) and may pose challenges on precision even for ambitious direct-imaging mission concepts (Gaudi et al. 2020).

The temperate sub-Neptune K2-18 b is a harbinger of the class of planets that might be habitable and exemplifies the need for a near-term method to measure the size of an H_2 atmosphere. The planet of 8.6 $M_\oplus$ and 2.6 $R_\oplus$ is in the habitable zone of an M dwarf star, and has a transmission spectrum (obtained by Hubble at 1.1–1.7 μm) with confirmed spectral features, which indicates that the planet should host an atmosphere dominated by H_2 (Benneke et al. 2019; Tsiaras et al. 2019). Interior structure models showed that the planet can have a massive (>∼1000 bar) H_2 atmosphere overlaying a rocky/Fe core and a possibly supercritical water layer, or a smaller (<100 bar) H_2 atmosphere with a water-dominated interior (Madhusudhan et al. 2020; Mousis et al. 2020; Nixon & Madhusudhan 2021). For K2-18 b, specifically, a ∼10–100 bar H_2 atmosphere overlaying a water layer would cause >200 bar of water to evaporate into the atmosphere, resulting in a hot steam atmosphere inconsistent with the observed transmission spectrum (Scheucher et al. 2020). An even smaller, ∼1 bar H_2 atmosphere would prevent this steam atmosphere and produce a liquid-water ocean (see Section 3), but this requires a very small rocky/Fe core and may be disfavored from the planet formation standpoint (e.g., Lee & Chiang 2016). However, a planet slightly more massive or smaller than K2-18 b—such as those at the center of the 1.7–3.5 $R_\oplus$ planet population—does not have this small-core difficulty to have a small atmosphere (Zeng et al. 2019; Nixon & Madhusudhan 2021), and many such planets and planet candidates have been detected and will soon be available for transmission spectroscopy (Figure 1, panel (a)).

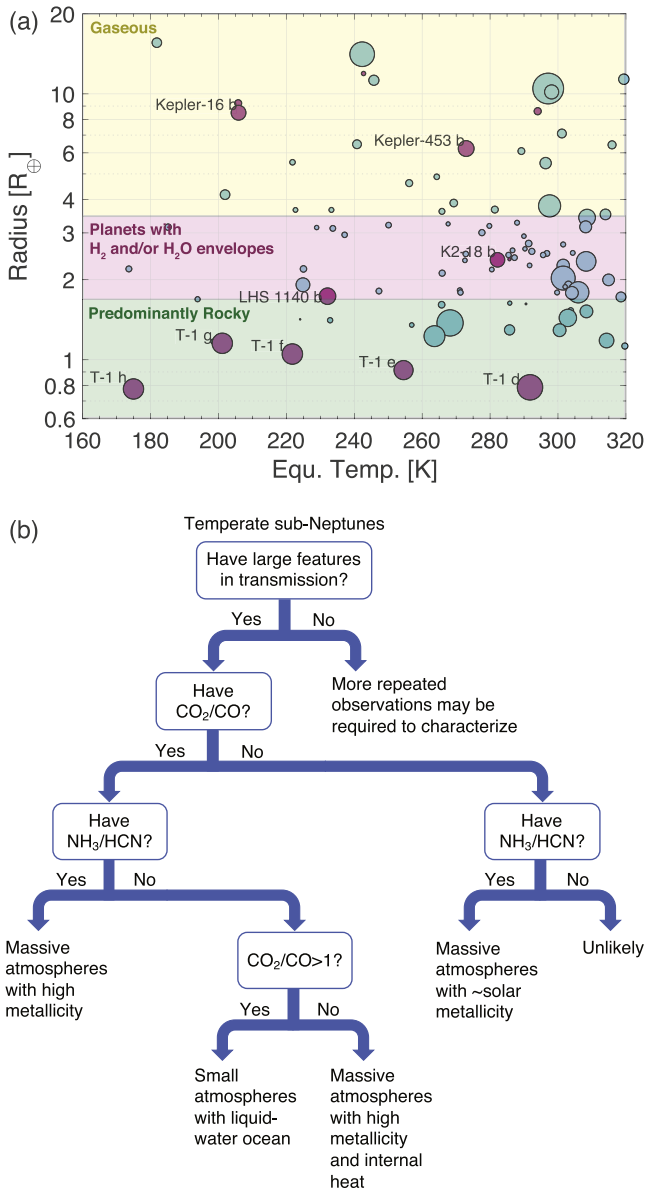

Figure 1. Temperate exoplanets amenable for atmospheric characterization via transmission spectroscopy. (a) Purple dots are confirmed planets with measured masses, and blue dots are planets with unknown masses or planet candidates. Data are taken from the NASA Exoplanet Archive and and the TESS Objects of Interest Catalog. The marker sizes are scaled with the expected signal-to-noise ratio of the spectral features of an H_2 atmosphere observed by JWST at 2 μm. Most of the temperate planets and planet candidates suitable for atmospheric characterization are larger than Earth and thus more likely to have H_2 atmospheres. (b) A roadmap to characterize the mass of the atmospheres and the habitability of temperate sub-Neptunes by detecting signature gases. See the text for details.

Here we propose that transit observations of temperate sub-Neptunes in the near- and mid-infrared wavelengths, which will soon commence with JWST, can detect small H_2 atmospheres that support liquid-water oceans and distinguish them from massive atmospheres (Figure 1, panel (b)). A companion paper has studied the atmospheric chemistry and spectral features of temperate planets with massive H_2 atmospheres (Hu 2021), and now we turn to temperate planets with small H_2 atmospheres. A recent paper might have similar intent as our work: Yu et al. (2021) studied the chemistry of temperate H_2 atmospheres with varied surface pressures, with assumed zero flux for all species at the lower boundary. The theories of Yu et al. (2021) may thus be more applicable to arid rocky planets without substantial volcanic outgassing, and here we instead focus on ocean planets, and address how to identify them observationally. As we will show later, a small atmosphere on a temperate sub-Neptune will have a distinctive composition because of its interaction with the ocean underneath.

2. Mutual Exclusivity of Habitability and Thermochemical Equilibrium

On temperate sub-Neptunes, the condition to form a liquid-water ocean and that to achieve the thermochemical equilibrium of carbon and nitrogen molecules are mutually exclusive. The CO_2–CO–CH_4 and N_2–NH_3 conversion rates are primarily a function of the temperature and to a lesser extent the pressure (Zahnle & Marley 2014; Tsai et al. 2018), and in a temperate sub-Neptune like K2-18 b, the thermochemical equilibrium of carbon and nitrogen molecules are typically achieved at the pressure of $10^7 \sim 10^8$ Pa, where the temperature is >1000 K (i.e., substantially higher than the critical point of water; Fortney et al. 2020; Hu 2021; Yu et al. 2021). Therefore, the gas-phase thermochemical equilibrium would be achieved in the deep and hot part of a massive atmosphere, and in contrast, it would not be achieved in a small atmosphere overlying a liquid-water ocean. Instead, NH_3 and sulfur species would be sequestered by the ocean (Loftus et al. 2019, and also see Section 3) and the abundance of CO_2 would be set by the ocean chemistry (Figure 2, with the cosmochemical and geological constraints detailed in the Appendix). This fundamental difference, coupled with atmospheric photochemistry, leads to distinctive gas abundances in the observable part ($<\sim$0.1 bar) of the atmosphere.

If the planet has a massive H_2 atmosphere, thermochemical reactions in the deep atmosphere recycle O, C, N, and S species into H_2O, CH_4, NH_3, and H_2S (Burrows & Sharp 1999; Heng & Tsai 2016; Blain et al. 2021; Woitke et al. 2021). H_2O can form a cloud and the above-cloud H_2O may be partially depleted as a result (Morley et al. 2014; Charnay et al. 2021; Hu 2021). Recent calculations have shown that the photodissociation of NH_3 in the presence of CH_4 leads to the formation of HCN and N_2, and that CO and CO_2 are produced by the photodissociation of CH_4 together with H_2O (Hu 2021). The photodissociation of H_2S leads to the formation of elemental sulfur haze (Hu et al. 2013; Zahnle et al. 2016), but the haze would likely be close to the cloud deck and would not mute transmission spectral features (Hu 2021). These photochemical products are transported to the deep atmosphere and recycled back to CH_4, NH_3, and H_2S. An exception is that planets with super-solar atmospheric metallicity and appreciable internal heat may have additional CO, CO_2, and N_2 transported from the deep troposphere and incomplete recycling to NH_3 (Fortney et al. 2020; Hu 2021; Yu et al. 2021).

If the planet instead has a small atmosphere and a liquid-water ocean, the thermochemical recycling cannot occur. Instead, CO_2 is the preferred form of carbon in equilibrium with a massive amount of H_2O (Hu & Seager 2014; Woitke et al. 2021), and NH_3 is dissolved in the ocean and largely depleted from the atmosphere (see Section 3). The abundance of atmospheric CO_2 is controlled by the oceanic pH (Kitzmann et al. 2015; Krissansen-Totton & Catling 2017; Isson & Planavsky 2018; Kite & Ford 2018) and that of N_2 is probably a combined result of the initial endowment and atmospheric escape. A reasonable lower bound of the total mass of CO_2 in the H_2 and H_2O layers can be derived from the

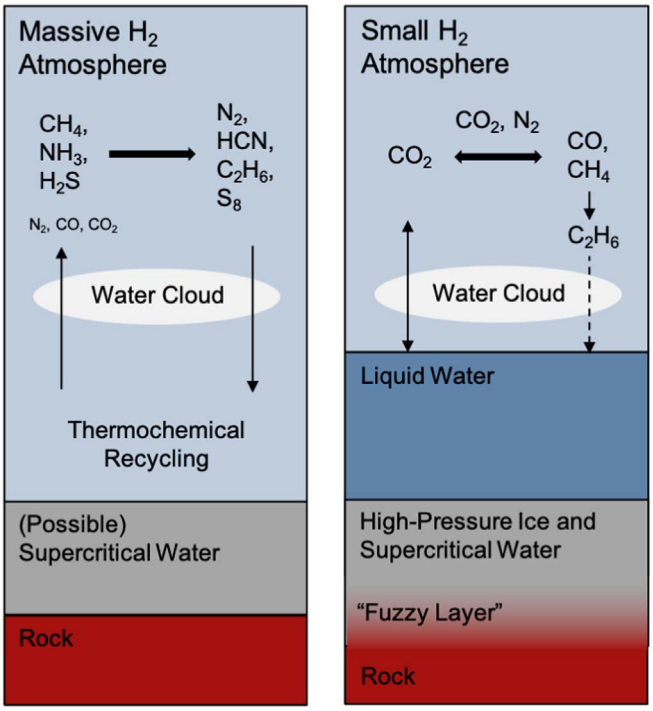

Figure 2. Interior structures of temperate H-rich exoplanets and the associated ranges of atmospheric composition. If the planet has a massive H_2 atmosphere, the deep atmosphere would be hot—enabling thermochemical recycling—but a liquid-water surface would not be possible. If the planet has a small H_2 atmosphere, a liquid-water surface may be possible. On these planets, the equilibrium abundance of atmospheric CO_2 is set by the oceanic chemistry and that of N_2 by atmospheric evolution.

cosmochemical constraints of planetary building blocks and the partitioning between the iron core, the silicate mantle, and the water layer (Appendix). Also, the "seafloor" of this thin-atmosphere, H_2O-rich sub-Neptune will not be a sharp interface in density and composition, but instead have a finite thickness (Vazan et al. 2020). The interface will be compositionally stratified with denser material underlying less dense material, and material transport across this "fuzzy layer" is inhibited due to the stratification. Thus, any carbon or nitrogen added to the H_2 and H_2O envelope by planetesimal accretion late in planet growth will remain in the envelope, and will not be stirred down into the silicate layer. Meanwhile, transit observations can straightforwardly identify H_2-dominated atmospheres and rule out CO_2- or N_2-dominated ones only from the size of spectral features (Miller-Ricci et al. 2008).

One might also consider the intermediate situation between massive atmospheres with thermochemical equilibrium and small atmospheres with liquid-water oceans, e.g., the atmospheres with a surface pressure from a few to ∼100 bars on K2-18 b. For many sub-Neptunes, this intermediate-atmosphere scenario would still require a massive water layer underneath to explain their mass and radius. If water was in the liquid form at the interface with the atmosphere, the evaporation of this ocean would make the atmosphere H_2O-dominated (Scheucher et al. 2020). If water is supercritical, any H_2 layer of intermediate mass should be well mixed with the water layer. Therefore, such an intermediate endowment of H_2 would most likely result in a non-H_2-dominated atmosphere, which is, again, distinguishable with transmission spectroscopy (Miller-Ricci et al. 2008).

3. Ocean Planet Models

We have used an atmospheric photochemical model (Hu et al. 2012) coupled with a radiative-convective model (Scheucher et al. 2020) to determine the steady-state abundances of photochemical gases in small and temperate H_2 atmospheres, for a cosmochemically and geologically plausible range of CO_2 abundance, and compared the compositions and transmission spectra with the massive H_2 atmosphere models published in Hu (2021). The massive-atmosphere models explored the atmospheric metallicity of 1–100× solar and included possible deep-tropospheric source CO, CO_2, and N_2 and incomplete recycling of NH_3 in super-solar atmospheres.

The photochemical model includes a comprehensive reaction network for O, H, C, N, and S species (including sulfur aerosols, hydrocarbons, and the reactions important in H_2 atmospheres), and it has been used to study the lifetime and equilibrium abundance of potential biosignature gases in H_2 atmospheres (Seager et al. 2013). We have updated the reaction network and tested the model with the measured photochemical gas abundance in the atmosphere of Jupiter (i.e., a low-temperature H_2 atmosphere; Hu 2021).

The pressure–temperature profiles (Figure 3) used as the basis for the photochemical model are calculated with the climate module of 1D-TERRA (Scheucher et al. 2020). The module uses a correlated-k approach with the random overlap method to include molecular absorption, collision-induced opacities, and the continuum of water vapor to calculate the radiative equilibrium, and the appropriate (moist or dry) adiabatic lapse rate to apply the convection adjustment. The module has been tested against the cases of Earth, Venus, and Mars, as well as with other radiative-convective and 3D climate models for modeling steam atmospheres (Scheucher et al. 2020).

As examples, we study H_2 atmospheres of 1 bar on a sub-Neptune planet that has a stellar irradiance similar to Earth and orbits around an early M star similar to K2-18. A 1 bar H_2 atmosphere on such a planet would likely have a surface temperature consistent with a liquid-water ocean (Figure 3). We adopt the "ocean-planet" interpretation of the 1.7–3.5 $R_\oplus$ planet population that centers at 10 $M_\oplus$, and 2.5 $R_\oplus$ (Zeng et al. 2019; Venturini et al. 2020), and assume 50% of water by mass in this study. In this interpretation, sub-Neptunes may be ocean planets with deep oceans that do not require a massive H_2 envelope to explain their radius, and can conceivably have moderate-size H_2 atmospheres. This may not be directly applicable for K2-18 b, which resides on the low-density side of the 1.7–3.5 $R_\oplus$ population. The specific choices of these parameters are, however, unimportant, because atmospheric chemistry is not sensitive to moderate changes in the surface gravity.

CO_2 is the main form of carbon in thermochemical equilibrium with H_2O (Hu & Seager 2014; Woitke et al. 2021). If a liquid-water ocean exists, the partial pressure of CO_2 is set by atmosphere-ocean partitioning, which in turn is mainly controlled by the oceanic pH (Kitzmann et al. 2015; Krissansen-Totton & Catling 2017; Isson & Planavsky 2018; Kite & Ford 2018). The pH is affected by the abundance of cations in the ocean, which come from complex water–rock reactions and dissolution of the seafloor. The rates of the processes involved are uncertain; therefore, we explore the mixing ratio of CO_2 from 400 ppm to 10%, corresponding to the pCO_2 range from the present-day Earth to early Earth

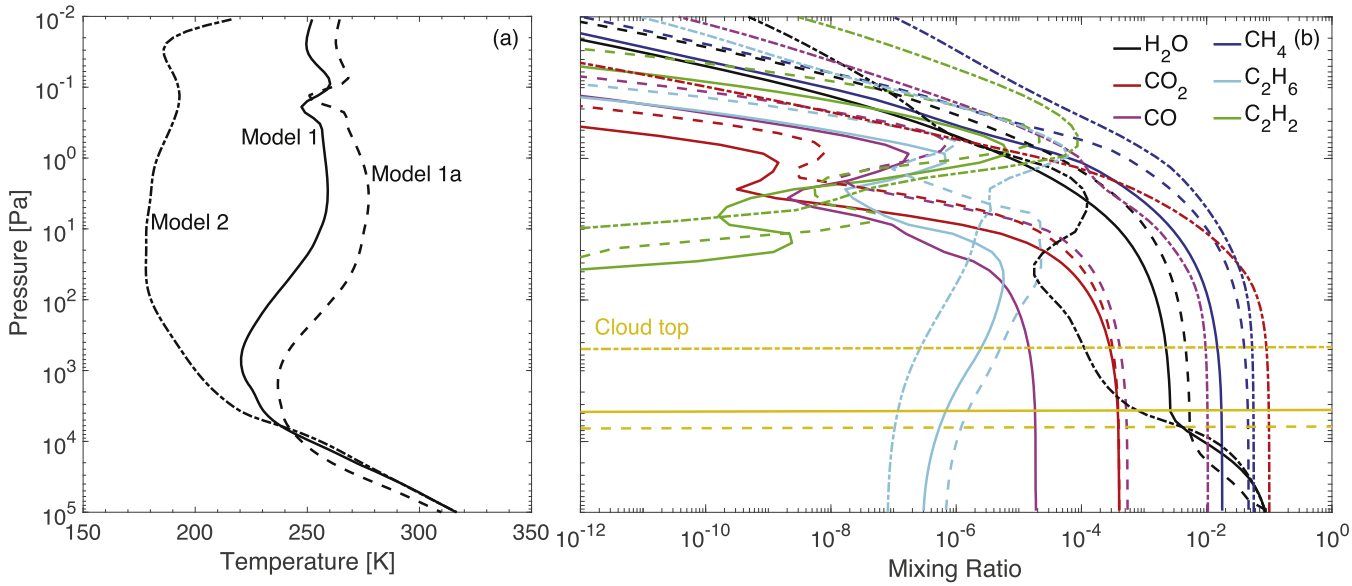

Figure 3. Modeled pressure–temperature profiles (a) and abundance profiles of main gases and photochemical products (b) in a temperate sub-Neptune like K2-18 b that has a small H_2 atmosphere. Solid, dashed, and dashed–dotted lines show the results for the low-CO_2 case (Model 1 in Table 1), the low-CO_2 case with additional CO sources (Model 1a), and the high-CO_2 case (Model 2). For the stellar irradiance, we use $S = S_{\rm Earth} * (1 - A_{\rm B})$, with a Bond albedo of $A_{\rm B} = 0.3$ (similar to Earth), to account for the radiative effects clouds would have in the otherwise cloud-free climate model. The surface albedo reflects a dark ocean (0.06). The surface temperatures in these models are consistent with a liquid-water ocean. The photochemical models use the UV spectrum of the M dwarf star GJ 176 (France et al. 2016; similar to K2-18; dos Santos et al. 2020). The steady-state mixing ratio CH_4 is high and those of nitrogen molecules such as NH_3 and HCN is $<10^{-12}$.

Table 1
Summary of the Photochemical Model Parameters and Results

Model	Name	CO_2	CO Flux	H_2O	CO	CH_4	C_2H_6
1	Low-CO_2	4×10^{-4}	0	2.3×10^{-3}	1.4×10^{-5}	1.5×10^{-2}	3.0×10^{-6}
1a	Low-CO_2 Variant	4×10^{-4}	1.0×10^{9}	3.3×10^{-3}	2.9×10^{-4}	2.9×10^{-2}	5.1×10^{-6}
2	High-CO_2	0.1	0	1.1×10^{-4}	9.5×10^{-3}	5.3×10^{-2}	4.0×10^{-7}

Note. The volume mixing ratio of CO_2 (as inputs) is at the lower boundary, and those of H_2O, CO, CH_4, and C_2H_6 (as results) are column-averaged in 10–10^3 Pa. The CO flux has a unit of $\rm cm^{-2}\,s^{-1}$.

(Catling & Kasting 2017) and including the predicted range for ocean planets (Kite & Ford 2018) that is still consistent with an H_2-dominated atmosphere. The 4×10^{-4} bar partial pressure of CO_2 in the low-CO_2 case, while not the absolute lower limit, is a cosmochemically and geologically reasonable lower bound of the CO_2 partial pressure on an ocean planet (Appendix).

The mixing ratio of N_2 on the modeled planet is probably set by atmospheric evolution (as opposed to the solubility equilibrium or geological recycling) and is assumed here to be 1%. As N_2 only minimally participates in the chemical cycles and does not have strong spectral features in the infrared, its exact abundance is not our main concern. The photochemical model indicates that the NH_3 produced by photodissociation of N_2 in H_2 atmospheres has negligible mixing ratios ($<10^{-12}$).

The pressure at the water–rock boundary of a $10 - M_\oplus$ and $2.5 - R_\oplus$ planet is ~500 GPa (Sotin et al. 2007; Levi et al. 2014), and this overloading pressure should suppress volcanism completely (Kite et al. 2009; Noack et al. 2017; Kite & Ford 2018). Therefore we do not include any volcanic outgassing in the standard models. As variant models, we consider the possibility of minor and intermittent sources of CO into the atmosphere. Evaporation of meteorites may provide a source of CO and CO_2 (Schaefer & Fegley 2017), and water–rock reactions at the temperature relevant to the "fuzzy layer" may produce CO (and not CH_4 as it is thermochemically disfavored at high temperatures). The rates of these processes are unknown, but numerical experiments with the photochemical model indicate that an additional CO source of 10^{10} molecule $\rm cm^{-2}\,s^{-1}$ would lead to a steady-state abundance of CO greater than that of H_2, effectively resulting in a CO-dominated atmosphere. A CO source of 10^9 molecule $\rm cm^{-2}\,s^{-1}$ would produce the CO-dominated atmosphere in the 10%-CO_2 case but not in the 400 ppm-CO_2 case. We therefore include a low-CO_2 case with the CO source of 10^9 molecule $\rm cm^{-2}\,s^{-1}$ as a variant model.

Table 1 summarizes the input parameters and results of the photochemical models, and Figure 3 shows the profiles of temperature and mixing ratios of main gases and photochemical products. CO is produced from the photodissociation of CO_2 and can build up to a 10^{-5} and 10^{-2} mixing ratio level for the low-CO_2 and the high-CO_2 cases. OH from the photodissociation of H_2O destroys CO and maintains its steady-state mixing ratio. CH_4 is also produced photochemically and can build up to a substantial mixing ratio ($10^{-3} \sim 10^{-2}$). This effectiveness in producing CH_4 from CO in temperate H_2 atmospheres has also been noted in Yu et al. (2021). Together with the high CH_4 mixing ratio, C_2H_6 is produced and can accumulate to a mixing ratio of $\sim 10^{-6}$. C_2H_2, as expected, is short-lived and only has significant mixing ratios in the upper

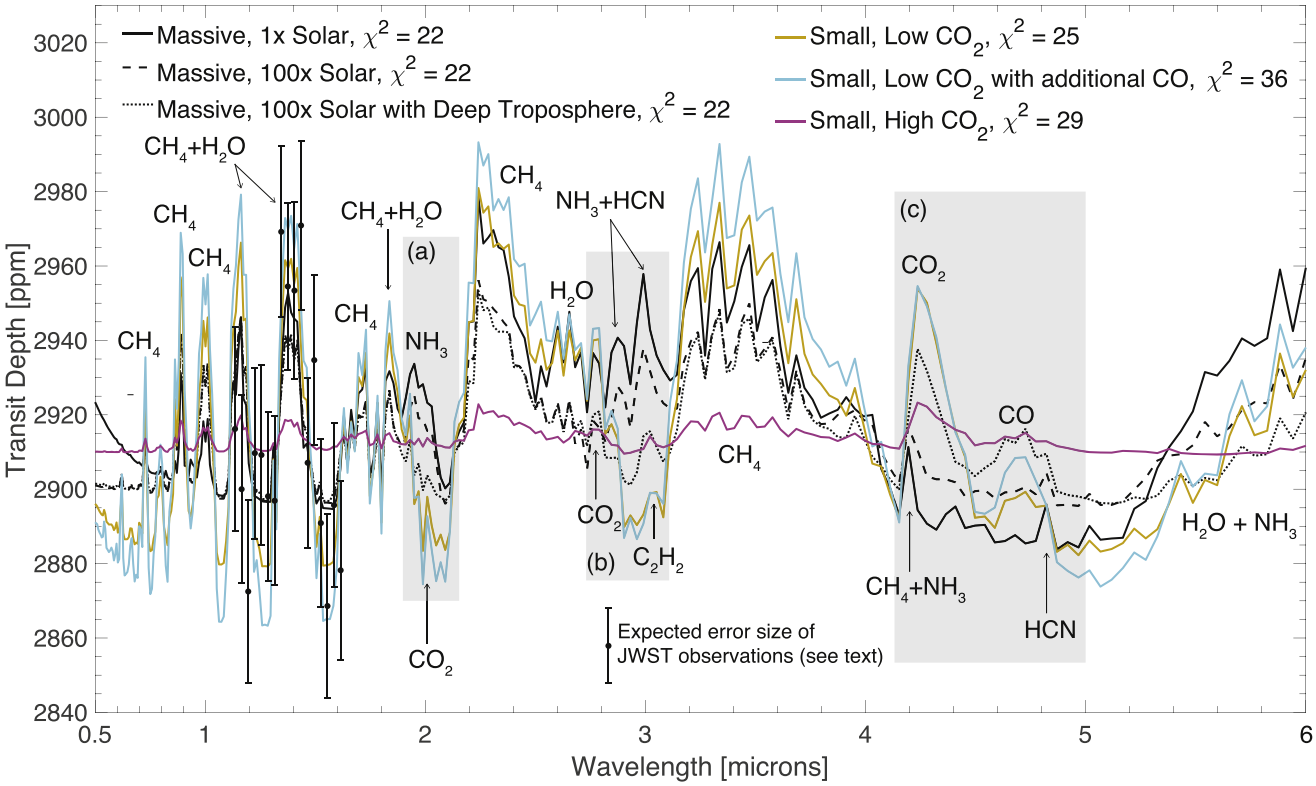

Figure 4. Modeled transmission spectrum of temperate sub-Neptune planets of M dwarf stars, using K2-18 b as an example and comparing with the planet's transit depth observed by Hubble (Benneke et al. 2019). The massive-H_2-atmosphere models (black lines) and the small-H_2-atmosphere models (colored lines) differ in three spectral regions: in (a) and (b), the massive-atmosphere models have absorption features of NH_3 and HCN, while the small-atmosphere models do not; in (c), the small-atmosphere models with a low mixing ratio of CO_2 (400 ppm) have prominent features of CO_2 and CO, while the massive-atmosphere models only have small features of NH_3 and HCN. The 100× solar massive atmosphere with deep-tropospheric source and sink may have subdued NH_3 and HCN features and prominent CO_2 and CO features. The small-atmosphere models with a high mixing ratio of CO_2 (10%) has a high mean molecular weight (∼6) and a high cloud top (Figure 3) and thus muted spectral features.

atmosphere. Here we have applied a deposition velocity of 10^{-5} cm s^{-1} for C_2H_6 to account for the loss of carbon due to organic haze formation and deposition (Hu et al. 2012); removing this sink does not substantially change the results shown in Figure 3. The additional source of CO would result in moderately more CO, CH_4, and C_2H_6 in the atmosphere (Model 1a in Table 1 and Figure 3). The photochemical CO and CH_4 can build up to the mixing ratio levels that cause significant features in the planet's transmission spectrum (Section 4).

Before closing this section, we address whether NH_3 can be produced substantially by water–rock reactions and then emitted into the atmosphere. Hydrothermal systems on early Earth may produce NH_3 from the reduction of nitrite and nitrate (Summers & Chang 1993; Summers 2005). On a planet with an H_2-dominated atmosphere, however, atmospheric production of the oxidized nitrogen including nitrite and nitrate should be very limited. Moreover, the storage capability of NH_3 by the ocean is vast and limits the emission into the atmosphere. At the pH value of 8 (a lower pH would further favor the partitioning of NH_3 in the ocean), 10^{-6} bar of atmospheric NH_3 requires a dissolved ammonium concentration of 10^{-3} mol l^{-1} in equilibrium (Seinfeld & Pandis 2016). The mass of NH_3 in the atmosphere and ocean is then $\sim 10^{-5}$ of the planetary mass. This would only be possible if much of the planet's rocky core begins with a volatile composition similar to carbonaceous chondrites, and most of this nitrogen is partitioned into the atmosphere and ocean as NH_3 (Marty et al. 2016), which is highly unlikely as N_2 is thermochemically favored. Therefore, the concentration of dissolved NH_3 should be small and so is the atmospheric NH_3 on a planet with a massive ocean.

4. Spectral Characterization

Figure 4 compares the expected spectra for the massive-atmosphere scenarios and the small-atmosphere scenarios. For K2-18 b, the massive-atmosphere models with 1–100× solar metallicity and the small-atmosphere models with a low mixing ratio of CO_2 (400 ppm) provide good fits to the transmission spectrum measured by Hubble.

Measuring the transmission spectra in an expanded wavelength range of 1–5 μm will distinguish the small atmospheres from massive ones. Using K2-18 b as an example for temperate sub-Neptunes, we see that the massive-atmosphere models and the small-atmosphere models, while having differences within each group, can be distinguished using the spectral regions of 1.9–2.1, 2.7–3.1, and 4.1–5.0 μm (the shaded areas a, b, and c in Figure 4). Both the massive-atmosphere and small-atmosphere models show spectral features of H_2O and CH_4, and so observing these two gases alone is unlikely to separate the massive versus small scenarios.

At 1.9–2.1 and 2.7–3.1 μm, the transmission spectra show NH_3 and HCN absorption in massive atmospheres but not in small atmospheres. If the 100× solar massive atmosphere has incomplete NH_3 recycling in the deep troposphere, it will have much weaker NH_3 and HCN features in these spectral regions. The transmission spectra of small atmospheres show small CO_2

features at ∼2.0 and ∼2.75 μm, but the feature at ∼2.75 μm is combined with a part of the H_2O feature with similar strength. The transmission spectra of small atmospheres also show a small C_2H_2 feature at ∼3.05 μm, and given enough precision, it might be distinguishable with the HCN feature at ∼3.0 μm.

At 4.1–5.0 μm, the transmission spectra of small atmospheres (the low-CO_2 cases) have prominent features of CO_2 and CO, while the spectra of massive atmospheres have weak features of NH_3 and HCN. If the 100× solar massive atmosphere has CO and CO_2 transported from the deep troposphere, it can have prominent spectral features of CO_2 and CO in this region as well.

From the above, we see that the 100× solar massive atmosphere with deep-tropospheric effects may resemble a small atmosphere in their transmission spectra (Figure 4), i.e., the lack of NH_3 or HCN and the prominence of CO_2 and CO. Would this potential "false positive" be avoidable? The answer may be yes given enough precision and spectral resolution. First, the spectrum of the massive atmosphere with deep-tropospheric effects still has weak spectral features of HCN, while none of the small atmospheres do. Second, the massive atmosphere has $CO_2/CO < \sim 0.1$, because CO always dominates over CO_2 in the deep H_2 troposphere of a temperate planet, and photochemical processes driven by an M dwarf star do not significantly raise the CO_2 mixing ratio in the observable part of the atmosphere (Hu 2021). In contrast, the small atmospheres typically have $CO_2/CO \geqslant 1$ (Table 1). In the more likely scenario without any volcanic outgassing, $CO_2/CO \sim 10$, because CO is produced photochemically from CO_2. Therefore, by measuring the abundance of CO and CO_2 independently, one could tell whether they are sourced from the deep troposphere.

Furthermore, a massive atmosphere with $\gg$100× solar metallicity will have a mean molecular weight much higher than that of an H_2 atmosphere and is thus also distinguishable by transmission spectroscopy.

With moderate time investment (i.e., <100 hr), JWST will provide the sensitivity to detect the signature gases aforementioned and distinguish massive versus small atmospheres on planets like K2-18 b. As an example, we have used PandExo (Batalha et al. 2017) to simulate the expected photometric precision using JWST's NIRSpec instrument. If combining two transit observations with NIRSpecs G235H grating and four transits with the G395H grating, the overall photometric precision would be ∼20 ppm per spectral element at a resolution of $R = 100$ in both channels that cover a wavelength range of 1.7–5.2 μm. These observations would distinguish the small-atmosphere scenarios versus the massive-atmosphere scenarios in Figure 4 with high confidence.

Additionally, we have performed spectral retrievals based on simulated observations using Tau-REx (Waldmann et al. 2015). We find that the mixing ratio of NH_3 and HCN and the lack of CO_2 or CO in the solar-abundance massive atmosphere would be usefully constrained (Figure 5). For the 100× solar atmosphere, the CO_2 and CO transported from the deep troposphere would be identified, and the posteriors suggest that CO is likely more abundant than CO_2. The reduction in the mixing ratios of NH_3 and HCN due to incomplete recycling could also be seen in the retrieval, although the constraints on the mixing ratio of HCN is not accurate. For the small atmosphere, the retrieval yields degenerate solutions and thus double peaks in some posterior distributions. Despite this, it is clear from the posteriors that the atmosphere likely has high mixing ratios of both CO_2 and CH_4, has more CO_2 than CO, and has very little NH_3 or HCN (Figure 5). In addition to JWST, the dedicated exoplanet atmosphere characterization mission ARIEL could also provide the sensitivity to detect these gases with more repeated transit observations (Changeat et al. 2020). This example shows that transit observations in the coming years can tell apart temperate sub-Neptunes with small H_2 atmospheres versus the planets with massive atmospheres and reveal their distinct atmospheric composition.

5. Discussion and Conclusion

Taken together, the results presented above identify a near-term path to detect small H_2 atmospheres that can be consistent with liquid-water oceans on temperate exoplanets. H_2 atmospheres are probably the only type of temperate atmospheres readily within the reach of JWST and ARIEL for detailed studies, since characterizing a heavier H_2O, N_2, or CO_2 atmosphere will require coadding a few tens of transits—something not impossible but probably very hard (Belu et al. 2011; Krissansen-Totton et al. 2018; Wunderlich et al. 2019; Pidhorodetska et al. 2020; Gialluca et al. 2021). The mass of the H_2 atmospheres—a parameter that is not directly measured by transits but critical for habitability if the planet is moderately irradiated—can be inferred from transmission spectra via the signature gases that indicate solubility equilibria versus gas-phase thermochemical recycling. The biggest uncertainty is probably the temperature at the 100 ∼ 1000 bar pressure level in the massive-atmosphere scenarios, which may be affected by heating mechanisms such as tidal heating. Detailed models of the interior temperature and mixing may further constrain this uncertainty (Fortney et al. 2020; Yu et al. 2021). Based on the range of the parameter space explored, we suggest that the sensitivity of multiple gases provided by future observatories' expanded wavelength coverage over Hubble would enable broad categorization of small versus massive atmospheres, summarized as a roadmap in Figure 1, panel (b).

How many sub-Neptunes could we expect to be ocean planets in the first place? The current population statistics of planets provide indirect evidence that most sub-Neptunes are not ocean planets (Owen & Wu 2017; Fulton & Petigura 2018; Jin & Mordasini 2018), but most known planets are hotter than planets that can be habitable. Even if the current statistics apply to temperate planets, there is plenty of room to have 10%–20% of sub-Neptunes be ocean planets, which will still be a lot of planets. Also, some planets in or just below the "radius valley" may be sub-Neptunes that have evolved into ocean planets (Kite & Schaefer 2021) and retained some residual H_2 (Misener & Schlichting 2021). For these reasons, this possibility of an ocean planet shrouded by a small H_2 atmosphere should motivate detailed observations of temperate planets with radius from near the "radius valley" (∼1.7 $R_\oplus$) to the main sub-Neptune population (∼2.5 $R_\oplus$). If some of the temperate planets in the aforementioned group have small H_2 atmospheres, their relative ease for transit observations would significantly enhance the prospect of detecting and characterizing potentially habitable exoplanets within the next decade.

The authors are thankful for helpful discussions with Fabrice Gaillard and Sukrit Ranjan. R.H. conceived and designed the study, simulated the photochemical models, interpreted the results, and wrote the manuscript. M.D. performed the JWST observation simulations and atmospheric retrievals. M.S. computed the pressure–temperature profiles. E.K. derived the

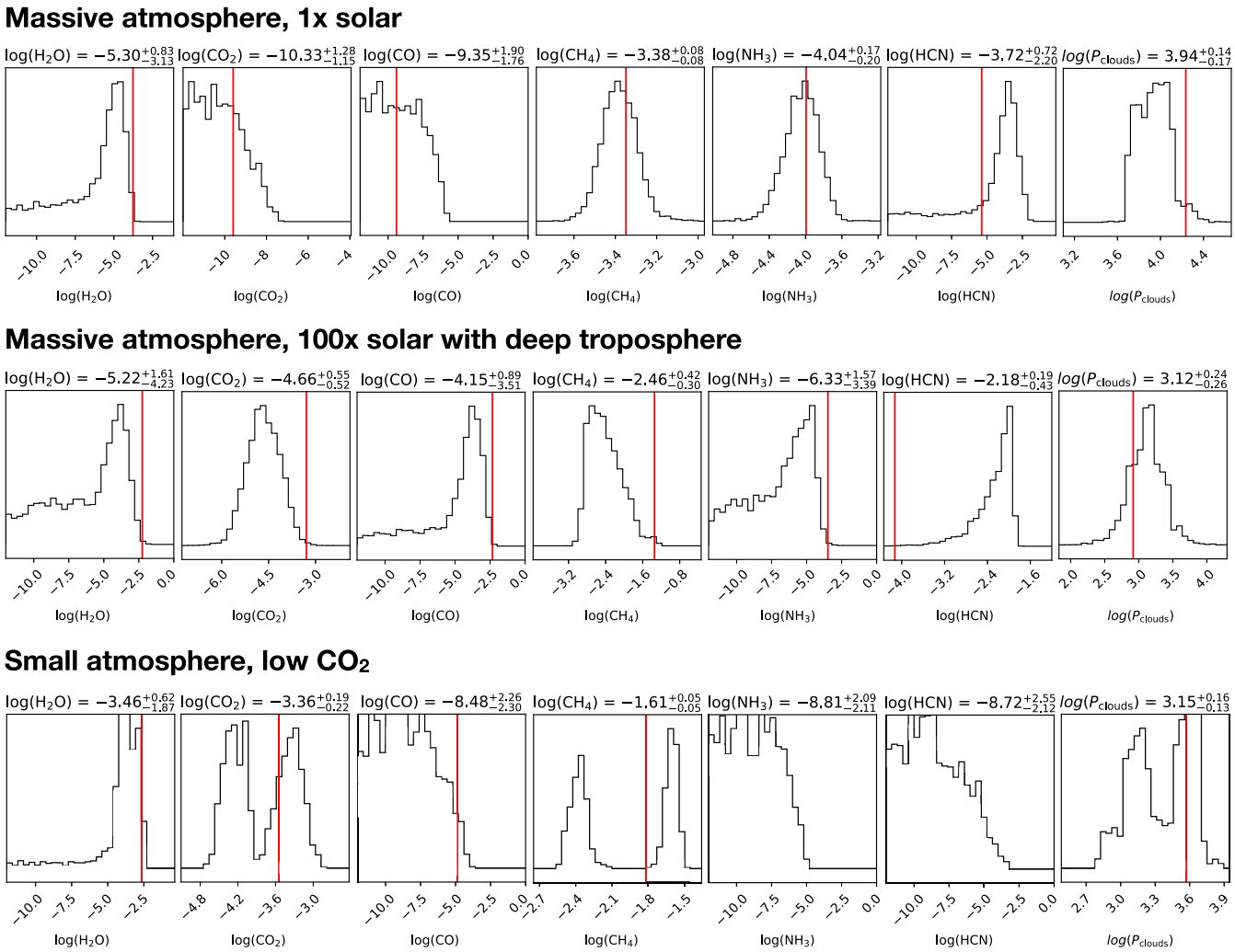

Figure 5. Retrieved posterior distributions of the abundances of the main chemical compounds and the cloud pressure in example massive-atmosphere and small-atmosphere scenarios. The input transmission spectra are calculated by Tau-REx using the atmospheric composition in Figure 3 and the expected uncertainties are calculated using PandExo (Batalha et al. 2017), assuming the combination of two transits of K2-18 b with NIRSpec/G235H and four transits with NIRSpec/G395H. The vertical red lines show the input value of the parameter, and the quantities on the top of each panel show the median and 1σ values summarized from the posterior. The cloud pressure ($P_{\rm clouds}$) has a unit of Pa. A detailed characterization of the atmosphere of K2-18 b, including distinguishing a small atmosphere vs. a massive one and measuring the abundances of H_2O, CH_4, NH_3, HCN, CO_2, and CO, will be achievable with moderate time investment of JWST.

cosmochemical and geological lower bounds for the carbon content. S.S. contributed interior structure models and insights. H.R. oversaw the development of the radiative-convective model used in the study. All authors commented on the overall narrative of the paper. The raw data that are used to generate the figures in this paper are available from the corresponding author upon reasonable request. This work was supported in part by NASA Exoplanets Research Program grant #80NM0018F0612. The research was carried out at the Jet Propulsion Laboratory, California Institute of Technology, under a contract with the National Aeronautics and Space Administration.

Appendix
Reasonable Lower Bound of CO_2

Is the 400 ppm CO_2, or 4×10^{-4} bar partial pressure in a 1 bar atmosphere, a reasonable lower bound of the CO_2 partial pressure on an ocean planet? We consider this question from a cosmochemical and geochemical perspective. Assuming equilibrium (during planet formation) between a Fe-core, a silicate mantle, and a well-mixed supercritical volatile envelope, the partitioning of C mass between reservoirs is described by

$$\mathrm{C_{total}} = \mathrm{C_{core}} + \mathrm{C_{silicate}} + \mathrm{C_{envelope}}, \tag{A1}$$

where all reservoir masses are in kilograms, and

$$\mathrm{C_{core}}/M_{\rm core} = D_{\rm C}(\mathrm{C_{silicate}}/M_{\rm silicate}), \tag{A2}$$

where $D_{\rm C}$ is a dimensionless partition coefficient, $M_{\rm core}$ (kg) is the mass of the Fe-dominated core, and $M_{\rm silicate}$ (kg) is the mass of the silicate mantle (molten during planet formation). For the partitioning between the envelope and the silicate mantle,

$$\mathrm{C_{envelope}} k (g_{\rm esi}/A_{\rm esi})(\mu_{\rm avg}/\mu_{\rm C}) s_{\rm C} = \mathrm{C_{silicate}}/M_{\rm silicate}, \tag{A3}$$

where k is a stochiometric correction from C mass to the mass of the C-bearing species in the envelope (i.e., $44/12 \sim 3.7$ for CO_2), $g_{\rm esi}$ is gravitational acceleration at the envelope-silicate interface in $\mathrm{m\,s^{-2}}$, $A_{\rm esi}$ is the area of the envelope-silicate interface in $\mathrm{m^2}$, $\mu_{\rm avg}$ is the average molecular weight of the envelope (in Da), $\mu_{\rm C}$ is the molecular weight of the C-bearing

species (in Da), and s_C is the solubility of the C-bearing species (in Pa^{-1}). Here we have assumed that the molten silicate layer is well-stirred.

Supposing $M_{core}/M_{silicate} \sim 0.5$ (like Earth) and $D_C \sim 10^3$ (Dasgupta 2013), then $C_{core}/C_{silicate} \sim 500$. If $C_{silicate}/M_{silicate} \sim 50$ ppm then $C_{core}/M_{core} \sim 2.5$ wt%, or $C_{total}/(M_{core} + M_{silicate}) \sim 1$ wt%, which is a reasonable lower bound for the primordial carbon endowment (see below). For $s_C = 0.55$ ppm Mpa^{-1} (Dasgupta & Grewal 2019), the envelope partial pressure of the C species ($=C_{envelope} k\ (g_{esi}/A_{esi})\ (\mu_{avg}/\mu_C)$) is $\sim 10^3$ bars. For a $5 - M_\oplus$ and $1.5 - R_\oplus$ core+mantle (Zeng et al. 2019) that defines the envelope-silicate boundary, and $\mu_{avg}/\mu_C = 0.4$ (appropriate for CO_2 in a H_2O-dominated supercritical layer during planet formation), the CO_2 mass in the envelope is 0.2% of an Earth mass. This estimate shows that even though most C is in the core, still-significant reservoirs of C exist both in the silicate and in the envelope (Bergin et al. 2015; Hirschmann 2016; Dasgupta & Grewal 2019; Keppler & Golabek 2019). Recent indications that the partition coefficient D_C is $\ll 10^3$ at the pressures and temperatures that are relevant for assembly of sub-Neptunes (Fischer et al. 2020) would imply even more envelope C enrichment.

Following the formation of the liquid-water ocean, almost all of the CO_2 will be dissolved in the ocean. For a $5 - M_\oplus$ water layer, the CO_2 mass in the envelope estimated above corresponds to a concentration of ~ 0.01 mol l^{-1} of dissolved CO_2. Here we have also assumed that the ocean is well-stirred. A higher oceanic pH leads to more effective dissolution and less CO_2 in the atmosphere. As an extreme, if cations are leached from the silicate and not charge-balanced by chloride ions, then an ocean composition with a pH of 9–10 ("a soda lake") will result (Kempe & Degens 1985). Using the equilibrium constant of carbonate and bicarbonate dissociation (Seinfeld & Pandis 2016), the CO_2 partial pressure in equilibrium with this ocean would be $5 \times 10^{-5} \sim 7 \times 10^{-4}$ bar, which is consistent with the assumed lower bound.

The partition coefficient gives the ratios of concentration of a species in the Fe-dominated core to the concentration of the same species in the silicate mantle. Therefore doubling the total amount of C in the core+mantle will double the concentration in the magma. What is the whole-planet C content? In principle, a planet can form without accreting volatiles. However, a thin-atmosphere sub-Neptune must have a thick volatile (H_2O) layer in order to match density data. It is very likely that a world that forms with tens of wt% H_2O will also accrete abundant C. We develop this point in more detail in the following paragraph.

At $T_{eff} \sim 300$ K, the minimum liquid-water content to explain most sub-Neptune masses and radii is $>\sim 50$ wt% even if there is no Fe-metal core (Mousis et al. 2020). This is more H_2O than can possibly be produced by hydrogen–magma reactions (Kite & Schaefer 2021), and instead implies a contribution of planet building blocks from the temperature range beyond the water ice snowline. This is a zone where (in the solar system) abundant refractory carbon is found. Specifically, the carbon content of primitive chondrite meteorites (CI and CM type) is 2–6 wt% (Pearson et al. 2006). Although we do not fully understand the origin of this refractory carbon, proposed mechanisms for forming this refractory carbon would also apply to exoplanetary systems (Bergin et al. 2014). Therefore we assume a planet bulk composition of (2–6 wt%) $\times (1 - x)$ carbon, where x is the H_2O mass fraction, and the remainder of the planet's building blocks are assumed to have C content similar to that of primitive chondrites. This is a conservative lower limit on bulk C content for a thin-H_2-atmosphere sub-Neptune, for the following two reasons. (i) It considers only refractory C, not C ices (e.g., CO_2 ice), which could be important in the case of whole-planet migration. (ii) Some primitive bodies in the solar system appear to be more C-rich than the most primitive chondrite meteorites; for example, the surface of the dwarf planet Ceres may contain 20 wt% C (Marchi et al. 2019). These large bulk C contents map to substantial envelope C contents (Equations (A1)–(A3)). As such, the 4×10^{-4} bar partial pressure of CO_2, while not the absolute lower limit, is a cosmochemically and geologically reasonable lower bound of the CO_2 partial pressure on an ocean planet.

ORCID iDs

Renyu Hu https://orcid.org/0000-0003-2215-8485
Mario Damiano https://orcid.org/0000-0002-1830-8260
Markus Scheucher https://orcid.org/0000-0003-4331-2277
Edwin Kite https://orcid.org/0000-0002-1426-1186
Sara Seager https://orcid.org/0000-0002-6892-6948
Heike Rauer https://orcid.org/0000-0002-6510-1828

References

Batalha, N. E., Mandell, A., Pontoppidan, K., et al. 2017, PASP, 129, 064501
Belu, A., Selsis, F., Morales, J.-C., et al. 2011, A&A, 525, A83
Benneke, B., Wong, I., Piaulet, C., et al. 2019, ApJL, 887, L14
Bergin, E., Cleeves, L. I., Crockett, N., & Blake, G. 2014, FaDi, 168, 61
Bergin, E. A., Blake, G. A., Ciesla, F., Hirschmann, M. M., & Li, J. 2015, PNAS, 112, 8965
Blain, D., Charnay, B., & Bézard, B. 2021, A&A, 646, A15
Burrows, A., & Sharp, C. 1999, ApJ, 512, 843
Catling, D. C., & Kasting, J. F. 2017, Atmospheric Evolution on Inhabited and Lifeless Worlds (Cambridge: Cambridge Univ. Press)
Changeat, Q., Edwards, B., Al-Refaie, A. F., et al. 2020, arXiv:2003.01486
Charnay, B., Blain, D., Bézard, B., et al. 2021, A&A, 646, A171
Cowan, N. B., Agol, E., Meadows, V. S., et al. 2009, ApJ, 700, 915
Dasgupta, R. 2013, RvMG, 75, 183
Dasgupta, R., & Grewal, D. S. 2019, in Deep Carbon: Past to Present, ed. B. Orcutt, I. Daniel, & R. Dasgupta (Cambridge: Cambridge Univ. Press), 4
dos Santos, L. A., Ehrenreich, D., Bourrier, V., et al. 2020, A&A, 634, L4
Fan, S., Li, C., Li, J.-Z., et al. 2019, ApJL, 882, L1
Fischer, R. A., Cottrell, E., Hauri, E., Lee, K. K., & Le Voyer, M. 2020, PNAS, 117, 8743
Fortney, J. J., Visscher, C., Marley, M. S., et al. 2020, AJ, 160, 288
France, K., Loyd, R. P., Youngblood, A., et al. 2016, ApJ, 820, 89
Fulton, B. J., & Petigura, E. A. 2018, AJ, 156, 264
Gaudi, B. S., Seager, S., Mennesson, B., et al. 2020, arXiv:2001.06683
Gialluca, M. T., Robinson, T. D., Rugheimer, S., & Wunderlich, F. 2021, PASP, 133, 054401
Heng, K., & Tsai, S.-M. 2016, ApJ, 829, 104
Hirschmann, M. M. 2016, AmMin, 101, 540
Hu, R. 2021, ApJ, 921, 27
Hu, R., & Seager, S. 2014, ApJ, 784, 63
Hu, R., Seager, S., & Bains, W. 2012, ApJ, 761, 166
Hu, R., Seager, S., & Bains, W. 2013, ApJ, 769, 6
Isson, T. T., & Planavsky, N. J. 2018, Natur, 560, 471
Jin, S., & Mordasini, C. 2018, ApJ, 853, 163
Kempe, S., & Degens, E. T. 1985, ChGeo, 53, 95
Keppler, H., & Golabek, G. 2019, Geochem. Perspect. Lett., 11, 12
Kite, E. S., & Ford, E. B. 2018, ApJ, 864, 75
Kite, E. S., Manga, M., & Gaidos, E. 2009, ApJ, 700, 1732
Kite, E. S., & Schaefer, L. 2021, ApJL, 909, L22
Kitzmann, D., Alibert, Y., Godolt, M., et al. 2015, MNRAS, 452, 3752
Koll, D. D., & Cronin, T. W. 2019, ApJ, 881, 120
Krissansen-Totton, J., & Catling, D. C. 2017, NatCo, 8, 15423
Krissansen-Totton, J., Garland, R., Irwin, P., & Catling, D. C. 2018, AJ, 156, 114
Lee, E. J., & Chiang, E. 2016, ApJ, 817, 90
Levi, A., Sasselov, D., & Podolak, M. 2014, ApJ, 792, 125
Loftus, K., Wordsworth, R. D., & Morley, C. V. 2019, ApJ, 887, 231

Madhusudhan, N., Nixon, M. C., Welbanks, L., Piette, A. A., & Booth, R. A. 2020, ApJL, 891, L7
Marchi, S., Raponi, A., Prettyman, T., et al. 2019, NatAs, 3, 140
Marty, B., Avice, G., Sano, Y., et al. 2016, E&PSL, 441, 91
Miller-Ricci, E., Seager, S., & Sasselov, D. 2008, ApJ, 690, 1056
Misener, W., & Schlichting, H. E. 2021, MNRAS, 503, 5658
Morley, C. V., Marley, M. S., Fortney, J. J., et al. 2014, ApJ, 787, 78
Mousis, O., Deleuil, M., Aguichine, A., et al. 2020, ApJL, 896, L22
Nixon, M. C., & Madhusudhan, N. 2021, MNRAS, 505, 3414
Noack, L., Rivoldini, A., & Van Hoolst, T. 2017, PEPI, 269, 40
Owen, J. E., & Wu, Y. 2017, ApJ, 847, 29
Pearson, V., Sephton, M., Franchi, I., Gibson, J., & Gilmour, I. 2006, M&PS, 41, 1899
Pidhorodetska, D., Fauchez, T. J., Villanueva, G. L., Domagal-Goldman, S. D., & Kopparapu, R. K. 2020, ApJL, 898, L33
Pierrehumbert, R., & Gaidos, E. 2011, ApJL, 734, L13
Ramirez, R. M., & Kaltenegger, L. 2017, ApJL, 837, L4
Robinson, T. D., Meadows, V. S., & Crisp, D. 2010, ApJL, 721, L67
Rogers, L., & Seager, S. 2010, ApJ, 716, 1208
Schaefer, L., & Fegley, B. 2017, ApJ, 843, 120
Scheucher, M., Wunderlich, F., Grenfell, J. L., et al. 2020, ApJ, 898, 44
Seager, S., Bains, W., & Hu, R. 2013, ApJ, 777, 95
Seinfeld, J. H., & Pandis, S. N. 2016, Atmospheric Chemistry and Physics: From Air Pollution to Climate Change (New York: Wiley)
Sotin, C., Grasset, O., & Mocquet, A. 2007, Icar, 191, 337
Summers, D. P. 2005, OLEB, 35, 299
Summers, D. P., & Chang, S. 1993, Natur, 365, 630
Tsai, S.-M., Kitzmann, D., Lyons, J. R., et al. 2018, ApJ, 862, 31
Tsiaras, A., Waldmann, I. P., Tinetti, G., Tennyson, J., & Yurchenko, S. N. 2019, NatAs, 3, 1086
Valencia, D., Guillot, T., Parmentier, V., & Freedman, R. S. 2013, ApJ, 775, 10
Vazan, A., Sari, R., & Kessel, R. 2020, arXiv:2011.00602
Venturini, J. E., Guilera, O. M., Haldemann, J., Ronco, M. P., & Mordasini, C. 2020, A&A, 643, L1
Waldmann, I. P., Tinetti, G., Rocchetto, M., et al. 2015, ApJ, 802, 107
Woitke, P., Herbort, O., Helling, C., et al. 2021, A&A, 646, A43
Wunderlich, F., Godolt, M., Grenfell, J. L., et al. 2019, A&A, 624, A49
Yu, X., Moses, J. I., Fortney, J. J., & Zhang, X. 2021, ApJ, 914, 38
Zahnle, K., Marley, M. S., Morley, C. V., & Moses, J. I. 2016, ApJ, 824, 137
Zahnle, K. J., & Marley, M. S. 2014, ApJ, 797, 41
Zeng, L., Jacobsen, S. B., Sasselov, D. D., et al. 2019, PNAS, 116, 9723